Comb-Based RF Photonic Filters Based on Interferometric Configuration and Balanced Detection

Hyoung-Jun Kim, Daniel E. Leaird, *Senior Member, IEEE*, Andrew J. Metcalf, *Student Member, IEEE*, and Andrew M. Weiner, *Fellow, IEEE*

***Abstract*—We demonstrate a novel technique to improve radio frequency (RF) performance such as RF gain and noise figure (NF) for comb-based RF photonic filters. While conventional RF photonic links use a dual-output modulator and balanced detection, this RF photonic filter utilizes an interferometric configuration with double sideband suppressed carrier modulation and balanced detection. This technique can simultaneously provide filter tunability, 6-dB RF gain increase, and noise cancellation. The RF gain and NF of the RF photonic filter are improved to approximately 0 and 24 dB, respectively. With the improved RF performance, we perform the tuning of the filter center frequencies from 2 to 8 GHz with no baseband filter response (<-38 dB), no RF power fading, while maintaining good filter shape (sidelobe suppression and stopband attenuation >32 dB).**

***Index Terms*—Finite impulse response filters, microwave photonics, optical combs, optical processing, programmable filters, tunable filters.**

I. Introduction

RADIO frequency (RF) filtering is an essential part of RF systems used in wireless communication, imaging, and sensing applications. Recently, with the demand for greater volume in broadband wireless service as well as increased data demands in high resolution imaging and sensing applications, the need for greater RF bandwidth has rapidly increased. In addition, the increased RF complexity required in applications such as software defined radio, cognitive radio, and multi-standard radio, can be simplified by using reconfigurable and multifunctional RF filters. However, it is difficult to tune traditional RF filter technologies rapidly over a large RF bandwidth and even more challenging to reconfigure them for different functionalities. As one example, yttrium iron garnet (YIG) filters have been widely used in various RF systems and provide wide tuning range, good selectivity, and good linearity. However, the tuning speed of the YIG filters is limited to the millisecond time scale [1]. The introduction of microelectromechanical systems (MEMS) variable capacitor approaches has led to recent advances in tunable RF filters [2]–[4]. The fundamental tuning speed of RF MEMS devices is characterized in [2] as limited to approximately 1–300 μs. Filters based on solid-state diodes have fundamentally higher tuning speeds but suffer from increased nonlinearity, loss, and power consumption [2]. In either of the latter technologies, challenges in controlling the coupled response of multiple resonances to maintain high filter selectivity practically constrain tuning to speeds much slower than the fundamental limits. Recent research has begun to go beyond frequency tuning to focus on reconfigurability. In one example, a second-order filter based on coupled evanescent-mode cavity resonators was used to demonstrate a bandstop-to-allpass reconfigurable filter [5]. Reconfiguration was accomplished via piezoelectric actuation of a flexible copper membrane. However, research into generally reconfigurable filters remains in its early stages, and rapid reconfiguration has not been explored.

RF photonics offers potential to implement filters that overcome these limitations. One approach utilizes a tapped delay line scheme [6]. Here, an RF-modulated optical signal is split to multiple branches which act as filter taps. Each of the branches has an optical attenuator and an optical delay line used to control the amplitude and phase of the RF signals, respectively. The split optical signals are then combined and detected by a photodiode to produce the RF waveform. The filter transfer function in this scheme can be characterized by a finite impulse response, allowing for the design of arbitrary amplitude filters. Furthermore, it is easy to process the wide-band RF signals due to a broad operational bandwidth of optical components such as optical attenuators and optical delay lines. However, it is not easy to implement these schemes with large number of filter taps. Other approaches utilize multi-wavelength sources [6]–[20]. In these schemes, RF-modulated multi-wavelength signals are transmitted through a single dispersive fiber or chirped fiber Bragg grating. Then differential delays between the multi-wavelength signals (i.e., filter taps) are applied through fiber dispersion. The amplitudes and delays of the filter taps can be controlled by adjusting the optical powers of the multi-wavelength signals and the length of the single dispersive fiber, respectively. Thus, this scheme also possesses a finite impulse response filter response and allows easy scaling of the filter taps by using various multi-wavelength sources. The above mentioned multi-channel sources have been realized in various ways, including an array of

Manuscript received January 15, 2014; revised May 7, 2014 and April 1, 2014; accepted May 11, 2014. Date of publication May 21, 2014; date of current version September 1, 2014. This work was supported in part by the Office of the Assistant Secretary of Defense for Research and Engineering under the National Security Science and Engineering Faculty Fellowship program under Grant N00244-09-1-0068 from the Naval Postgraduate School. Any opinion, findings, and conclusions or recommendations expressed in this publication are those of the authors and do not necessarily reflect the views of the sponsors.

The authors are with the School of Electrical and Computer Engineering, Purdue University, West Lafayette, IN 47907-2035, USA (e-mail: sjun27@purdue.edu; leaird@purdue.edu; metcalfa@purdue.edu; amw@purdue.edu).

Color versions of one or more of the figures in this paper are available online at http://ieeexplore.ieee.org.

Digital Object Identifier 10.1109/JLT.2014.2326410

continuous-wave laser sources [7], [8], spectrally sliced broadband light sources [9], [10], and optical frequency combs such as mode-locked lasers [11] and electro-optically (EO) generated combs [12]–[20]. Among these sources, the EO-generated combs are very attractive for RF photonic filtering and other RF photonic signal processing due to their spectral flatness, high coherence, tunable repetition rate, and good stability [21], [22]. Our group has previously demonstrated reconfigurable RF photonic filters using an EO-generated comb and pulse shaper in an interferometric configuration [12]–[16]. Gaussian bandpass filters with fast ($\sim$40 ns) tunability of the passband center frequency, high sidelobe suppression radio ($>$60 dB), and high stopband attenuation ($>$70 dB) were demonstrated in [15]. Reconfigurable flat-topped filters were reported in [14]. In [16] and [18], reconfigurable phase filters were implemented and applied for compression of wideband RF chirp signals. Using a similar comb-based RF filter configuration but without the interferometer, rapid ($\sim$20 ns) bandwidth reconfiguration was demonstrated in [19], and simultaneous tunable bandpass filtering and downconversion was reported in [20]. Thus, such comb-based RF photonic filters offer a degree of reconfigurability far beyond what is currently available from other technologies, as well potential for extremely fast tuning and reconfigurability.

To date, however, such RF photonic filters have typically performed poorly in terms of RF gain and noise. In [15] for example, the typical RF gain was limited to approximately -40 dB at 0.5 mA photocurrent. In this and other RF photonic filter schemes, the output photocurrent can be increased by the use of erbium-doped fiber amplifiers (EDFAs) to increase the RF gain. However, the EDFA also amplifies the intensity noise of the comb sources and generates amplified spontaneous emission noise, resulting in a very poor noise figure (NF).

Although RF performance metrics such as RF gain and NF have been studied extensively in research on conventional RF photonic links [23]–[25], such metrics have seldom been considered in the context of reconfigurable RF photonic filtering. Balanced (or differential) detection is a well known approach to mitigate noise problems in RF photonic links. Demonstrations such as those reported in [24] and [25] utilized a dual-output modulator and balanced photodetector (BPD) to suppress common mode intensity noise while increasing photocurrent by a factor of two (increasing RF gain by 6 dB). In [24], the reported RF gain and NF were $>$17 dB and $<$6.5 dB across 6–12 GHz, respectively.

One interesting recent theoretical paper [26] does analyze the gain, noise, and intermodulation distortion of RF photonic links extended to include filtering action in a rather general way. However, the specific tunable RF photonic filter implementation of interest in the current work, in which a modulator is embedded in one arm of an optical interferometer, does not appear to be captured within the configuration assumed in [26]. A few recent experimental papers have reported RF photonic filters using incoherent broadband light sources and BPDs [27]–[30]. However, the focus of these papers was on filter reconfigurability; RF gain and NF were not evaluated.

In this paper we seek to demonstrate substantial experimental improvement in the RF performance of comb-based RF photonic filters by incorporating balanced photodetection into the interferometric configuration our group previously introduced to enable tuning in such filters [12]–[16]. Instead of using a dual-output modulator, we utilize double sideband suppressed carrier (DSB-SC) modulation in one arm of the interferometer. This innovative configuration simultaneously provides 6 dB RF gain increase, while improving noise performance, supporting tunability, and eliminating unwanted baseband response. Furthermore, we show that optimizing the input split ratio at the interferometer improves both the effective optical modulation index and the NF. Here, the interferometer splits the input into two paths which we refer to as the delay and modulation paths. As the fractional power split to the delay path decreases, both RF gain and total output noise are also decreased. However, because the total output noise decreases more rapidly than the RF gain, the NF is reduced. This principle is analogous to low-biasing, a common noise reduction technique in RF photonic links [23], [24]; to the best of our knowledge, our work is the first extension of this principle to RF photonic filtering. Another feature of our work concerns our treatment of the long dispersive fiber needed to realize filtering action. Unlike conventional RF photonic links, where double-sideband modulation leads to RF fading upon dispersive propagation, in the interferometric filter scheme, such RF power fading does not occur [12]. However, one must address the challenge of providing stable and closely matched dispersive links to each of the photodetectors. Here we investigate two schemes which achieve simultaneous dispersion and time delay matching, namely, bidirectional propagation [28], [29] and polarization multiplexing [30]. Our current work focuses on RF gain and NF; the important topics of nonlinear distortion and dynamic range are left for future study.

A preliminary description of our results was published in [31]. Here in a substantially expanded discussion, we report the full theoretical development for the first time and include a new experiment which achieves further improvement in RF gain and NF while simultaneously tuning from 2 to 8 GHz.

The remainder of this paper is organized as follows. Section II describes the concept of this RF photonic filter and derives its RF performance metrics such as RF gain and NF. In Section III, we simulate the effect of the input split coefficient of the interferometer on the RF performance. In Section IV, we experimentally investigate the RF performance improvements of our BPD scheme compared to the performance obtained using a single photodetector (SPD). In an initial static filtering experiment, we obtain RF gain and NF of -10 and 29 dB. The use of a BPD provides improvements of 6 and 21 dB, respectively, compared to SPD operation [31]. We also report new data that reveal significant contributions to the noise due to Brillouin scattering effects in the bidirectional propagation geometry employed. Then, in a new experiment in which we use a lower-V_π IM, increase the output photocurrent, and switch to a polarization multiplexing geometry, we further improve the RF performance, demonstrating RF gain and NF of 0 and 24 dB, respectively. While tuning the filter passband across the 2 to 8 GHz range, the maximum variation of the RF gain and NF are 1.3 and 2 dB, respectively. Finally, in Section V, we conclude.

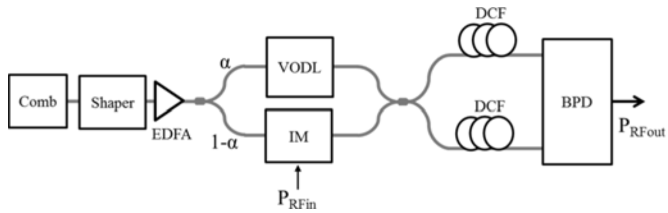

Fig. 1. Concept of comb-based microwave photonic filters using the interferometric configuration with double sideband suppressed carrier and balanced detection. EDFA: erbium-doped fiber amplifier; VODL: variable optical delay line; IM: intensity modulator; DCF: dispersion compensating fiber; BPD: balanced photodetector.

II. Concept and Theory

A. Concept

Fig. 1 shows a conceptual diagram of RF photonic filters in an interferometric configuration utilizing DSB-SC and a BPD. The EO-generated comb, which is nearly flat, is first sent through an optical pulse shaper. The pulse shaper is used to carve out a Gaussian-shaped spectrum from the input source in order to provide a good filter shape in the RF domain. The resulting Gaussian-shaped comb is amplified by the EDFA and directed to the interferometer. In the delay path (i.e., upper path), a variable optical delay line is used to tune the center frequency of the filter passband [12]–[15]; in the modulation path (i.e., lower path), a DSB-SC IM, biased at a minimum transmission point, is used [12], [32]. This results in suppression of the optical carriers and intensity noise in the modulation path. The interferometer output signals are directed through the dispersion compensating fiber (DCF) stage and input to the BPD, which acts to suppress the intensity noise from the delay path. Although two identical DCFs are pictured in the figure, in experiments we use a single DCF configuration with either bidirectional propagation or polarization multiplexing, discussed in more detail later. Ideally, the intensity noise originating from common mode signal-spontaneous beat noise can be perfectly suppressed through the combination of the interferometric configuration with the DSB-SC and balanced detection. However, the finite extinction ratio value of the IM causes non-common mode signal-spontaneous beat noise which is generated by the beating of the optical carriers in one arm with the intensity noise in the other arm. We will refer to the non-common mode signal-spontaneous beat noise due to the finite extinction ratio of the IM as excess noise. The residual common mode noise due to a finite common mode rejection ratio of the BPD is negligible when the two DCF paths are well balanced. The spontaneous-spontaneous beat noise is also negligible, compared to the signal-spontaneous beat noise.

B. Derivation of RF Performance Metrics

We derive the output photocurrent of the RF signal from the electric field of the optical frequency comb in order to describe the filter transfer function and RF gain. Then, the output noise power spectral density (PSD) is derived in order to describe the NF.

The electric field of the optical frequency comb at the output of the EDFA can be written as

$$e_{\mathrm{comb}}(t) = \sum_n \sqrt{p_n \alpha_S g_A}\,\mathrm{e}^{j\omega_n t} + \mathrm{c.c} \tag{1}$$

where p_n and ω_n are the optical power and angular frequency of the *n*th comb line, respectively, where we have used c.c. to represent the complex conjugate of the first term on the right side. The angular frequencies satisfy $\omega_n = \omega_0 + n\Delta\omega$. ω_0 and $\Delta\omega$ are the angular frequency of the optical carrier and comb spacing (i.e., repetition rate), respectively. α_s is the optical loss factor of the pulse shaper. g_A is the optical gain factor of the EDFA. An electrical RF signal drives the IM which is biased at the minimum transmission point. We write the electrical RF signal at the input of the IM as

$$\nu_{\mathrm{in}}(t) = V_{\mathrm{rf}}\cos(\omega_{RF} t) \tag{2}$$

where V_{rf} and ω_{RF} are the RF voltage and angular RF frequency, respectively. By taking the small signal approximation, the electric field at the IM output [33] can be written as

$$e_{IM}(t) = \frac{\sqrt{\alpha_M}\, e_{\mathrm{in}}(t)}{2} \times \left[2\sqrt{\varepsilon} - j\frac{\pi V_{\mathrm{rf}}}{2V_\pi}e^{j\omega_{RF}t} - j\frac{\pi V_{\mathrm{rf}}}{2V_\pi}e^{-j\omega_{RF}t}\right] + \mathrm{c.c} \tag{3}$$

where $e_{\mathrm{in}}(t)$ is the electric field at the IM input. α_M and ε are the optical loss factor and extinction ratio of the IM, respectively. The first term represents the residual optical carriers which are incompletely suppressed due to the modulator's finite extinction ratio. The other terms represent the two optical sidebands. We write the electric fields at the two outputs of the interferometer as

$$e_A(t) = \sum_n \sqrt{p_n \alpha_S g_A} \times \left[\begin{array}{l} \left(\sqrt{\frac{\alpha}{2}\alpha_D}\, e^{-j\omega_n \tau} - \sqrt{\frac{(1-\alpha)\varepsilon\alpha_M}{2}}\right)\mathrm{e}^{j\omega_n t} \\ +j\frac{\pi V_{\mathrm{rf}}\sqrt{(1-\alpha)\alpha_M}}{4\sqrt{2}V_\pi} e^{j(\omega_n+\omega_{RF})t} \\ +j\frac{\pi V_{\mathrm{rf}}\sqrt{(1-\alpha)\alpha_M}}{4\sqrt{2}V_\pi} e^{j(\omega_n-\omega_{RF})t} \end{array}\right] + \mathrm{c.c} \tag{4}$$

$$e_B(t) = \sum_n \sqrt{p_n \alpha_S g_A} \times \left[\begin{array}{l} \left(j\sqrt{\frac{\alpha}{2}\alpha_D}\, e^{-j\omega_n \tau} + j\sqrt{\frac{(1-\alpha)\varepsilon\alpha_M}{2}}\right)\mathrm{e}^{j\omega_n t} \\ +\frac{\pi V_{\mathrm{rf}}\sqrt{(1-\alpha)\alpha_M}}{4\sqrt{2}V_\pi} e^{j(\omega_n+\omega_{RF})t} \\ +\frac{\pi V_{\mathrm{rf}}\sqrt{(1-\alpha)\alpha_M}}{4\sqrt{2}V_\pi} e^{j(\omega_n-\omega_{RF})t} \end{array}\right] + \mathrm{c.c} \tag{5}$$

where α is the fraction of the power directed toward the upper arm of the interferometer (the delay path), α:$1-\alpha$ is the input power split ratio of the interferometer, τ is the delay difference between the two paths of the interferometer, and α_D is the optical loss factor of the variable optical delay line. A symmetric 3 dB coupler is assumed to form the interferometer output. After propagation through the DCF, we write the electric fields at the two inputs of the BPD as

$$e_{\mathrm{BPD}-A}(t) = \sum_n \sqrt{p_n \alpha_S g_A \alpha_F} \times \begin{bmatrix} \left(\sqrt{\frac{\alpha}{2}\alpha_D} e^{-j\omega_n \tau} - \sqrt{\frac{(1-\alpha)\varepsilon\alpha_M}{2}}\right) \mathrm{e}^{j[\omega_n t + \psi(\omega_n)]} \\ +j\frac{\pi V_{\mathrm{rf}}\sqrt{(1-\alpha)\alpha_M}}{4\sqrt{2}V_\pi} \mathrm{e}^{j[(\omega_n + \omega_{RF})t + \psi(\omega_n + \omega_{RF})]} \\ +j\frac{\pi V_{\mathrm{rf}}\sqrt{(1-\alpha)\alpha_M}}{4\sqrt{2}V_\pi} e^{j[(\omega_n - \omega_{RF})t + \psi(\omega_n - \omega_{RF})]} \end{bmatrix} + \mathrm{c.c} \tag{6}$$

$$e_{\mathrm{BPD}-B}(t) = \sum_n \sqrt{p_n \alpha_S g_A \alpha_F} \times \begin{bmatrix} \left(j\sqrt{\frac{\alpha}{2}\alpha_D} e^{-j\omega_n \tau} + j\sqrt{\frac{(1-\alpha)\varepsilon\alpha_M}{2}}\right) \mathrm{e}^{j[\omega_n t + \psi(\omega_n)]} \\ +\frac{\pi V_{\mathrm{rf}}\sqrt{(1-\alpha)\alpha_M}}{4\sqrt{2}V_\pi} \mathrm{e}^{j[(\omega_n + \omega_{RF})t + \psi(\omega_n + \omega_{RF})]} \\ +\frac{\pi V_{\mathrm{rf}}\sqrt{(1-\alpha)\alpha_M}}{4\sqrt{2}V_\pi} e^{j[(\omega_n - \omega_{RF})t + \psi(\omega_n - \omega_{RF})]} \end{bmatrix} + \mathrm{c.c} \tag{7}$$

where α_F is the optical loss factor of the dispersive media and $\psi(\omega)$ is the quadratic phase introduced by the chromatic dispersion [34] given by

$$\psi(\omega) = -\beta(\omega) L = \psi_0 + \psi_1(\omega - \omega_0) + \frac{\psi_2}{2}(\omega - \omega_0)^2 \tag{8}$$

where the dispersion coefficient ψ_2 relates to the dispersion parameter D (in ps/nm/km) as

$$\psi_2 = \frac{D\lambda^2 L}{2\pi c}. \tag{9}$$

The photocurrent at the BPD output is given by

$$i(t) = \kappa_B \left\langle |e_{\mathrm{BPD}-B}(t)|^2 \right\rangle - \kappa_A \left\langle |e_{\mathrm{BPD}-A}(t)|^2 \right\rangle \tag{10}$$

where κ_A and κ_B are the responsivities of the BPD, which in the following are taken to be equal ($\kappa = \kappa_A = \kappa_B$), and $\langle\rangle$ stands for averaging over the optical oscillations. We write the output photocurrents of the RF signal as shown (11), at the bottom of the next page.

The filter transfer function, giving the ratio of the output RF voltage to the input RF voltage, can be written as

$$H(\omega_{RF}) \propto \frac{\pi\kappa\alpha_F \alpha_S g_A R\sqrt{\alpha(1-\alpha)\alpha_D\alpha_M}}{2V_\pi} \begin{Bmatrix} \mathrm{e}^{j\left[\omega_0\tau + \frac{\psi_2}{2}\omega_{RF}^2\right]} \sum_n p_n \mathrm{e}^{j[n\Delta\omega(\psi_2\omega_{RF} + \tau)]} \\ -\mathrm{e}^{-j\left[\omega_0\tau + \frac{\psi_2}{2}\omega_{RF}^2\right]} \sum_n p_n \mathrm{e}^{j[n\Delta\omega(\psi_2\omega_{RF} - \tau)]} \end{Bmatrix} \tag{12}$$

where R is the impedance of the photodetectors. In this expression we have omitted phase prefactors. The two terms within the brackets comprise two different filter passbands, one arising from each of the modulation sidebands [12]. The filter transfer functions depend on the Fourier transform of the shaped optical comb spectrum and are periodic with free spectral range (FSR) given (in Hz units) by $\mathrm{FSR} = 1/\psi_2\Delta\omega = 1/\mathrm{T}$, where T is the differential delay between the filter taps. The center frequencies of the two passbands are shifted in opposite directions when the delay difference between the two paths of the interferometer is changed. Thus, there is no RF power fading because the two filter passbands are not overlapped [12]. We write the RF gain at the center RF frequency of the filter passbands, derived from (11), as

$$G_{\mathrm{rf}} = \frac{P_{\mathrm{out}}}{P_{\mathrm{in}}} = \left(\frac{\pi\kappa p_S \alpha_S g_A \alpha_F \sqrt{\alpha(1-\alpha)\alpha_D\alpha_M} R}{2V_\pi}\right)^2. \tag{13}$$

where $p_s = \sum_n p_n$ is the total comb power. We rewrite the RF gain in terms of the total output dc photocurrent (I_{DC}), which is the sum of the photocurrents in each of two photodiodes of the BPD, and the ratio (η) of the loss factor in the modulation path of the interferometer to the loss factor in the delay path as

$$G_{\mathrm{rf}} \approx \left[\frac{1}{4}\frac{\eta}{\varepsilon[1+\eta]^2}\left(\frac{\pi I_{\mathrm{DC}} R}{V_\pi}\right)^2\right] \tag{14}$$

where I_{DC} and η are given by

$$I_{\mathrm{DC}} \approx p_s \alpha_s g_A \left[\alpha\alpha_D + (1-\alpha)\varepsilon\alpha_M\right] \alpha_F \kappa \tag{15}$$

and

$$\eta = \frac{(1-\alpha)\varepsilon\alpha_M}{\alpha\alpha_D}. \tag{16}$$

The total output noise PSD (N_{out}) [35] can be written as

$$N_{\mathrm{out}} = (1 + G_{\mathrm{rf}})N_{\mathrm{th}} + N_{\mathrm{shot}} + N_{ex} \tag{17}$$

where $N_{\mathrm{th}} = \mathrm{kT}$ represents the thermal noise (k is Boltzmann's constant), $N_{\mathrm{shot}} = 2\mathrm{qI_{DC}R}$ is the shot noise, and N_{ex} is the excess noise. As mentioned in the previous section, the excess noise is dominated by signal-spontaneous beat noise. In our configuration each optical comb line gives rise to four distinct beat noise contributions at RF frequency ω_{RF}: the beating of the optical carrier (ω_n) from the delay path with the residual optical noise at each of frequencies ($\omega_n + \omega_{RF}$ and $\omega_n - \omega_{RF}$) transmitted through the modulation path, and the beating of the optical noise at frequencies $\omega_n + \omega_{RF}$ and $\omega_n - \omega_{RF}$ from the delay path with the residual carrier transmitted through the modulation path. The excess noise is calculated as

$$N_{ex} = \sum_n \begin{pmatrix} 32\left(\frac{\alpha\alpha_D\alpha_F}{2}\right)\left(\frac{(1-\alpha)\varepsilon\alpha_M\alpha_F}{2}\right) p_n\alpha_S g_A \rho_n \kappa^2 R \\ \left[\cos^2\left(\omega_n\tau + \frac{\omega_{RF}\tau}{2}\right) + \cos^2\left(\omega_n\tau - \frac{\omega_{RF}\tau}{2}\right)\right] \end{pmatrix} \tag{18}$$

where the first and second terms in parentheses inside the summation represent the transmission factors associated with upper and lower interferometer paths, respectively, including also the subsequent dispersive fiber propagation, and $p_n\alpha_S g_A$ is the power of the $\mathrm{n^{th}}$ comb line at the input to the interferometer. ρ_n is the PSD of the optical noise in the vicinity of the $\mathrm{n^{th}}$ comb line frequency at the output of the EDFA (input to the interferometer) and is assumed to be polarized. One cosine squared term in (18) arises due to the interferometric combination of the two RF beat terms involving the optical noise at frequency $\omega_n + \omega_{RF}$; the other arises due to the interferometric combination of the two terms involving the optical noise at frequency $\omega_n - \omega_{RF}$. With summation over a large number of comb lines, it can be shown that the cosine squared terms each average nicely to a value of approximately 0.5 for most cases. (The exception is for settings of the interferometer delay τ very close to $n\pi/\Delta\omega$, where *n* is an integer in this range the cosine squared terms vary rapidly with τ, even after summation.) Taking each of the cosine squares as 0.5, the excess noise derived from the electric field of the optical comb and noise PSD can be written as

$$N_{ex} \approx 8R\left(\kappa\alpha_F\right)^2 \alpha\alpha_D(1-\alpha)\varepsilon\alpha_M \sum_n \rho_n p_n \alpha_S g_A. \quad (19)$$

We can rewrite the excess noise with I_{DC} and η as

$$N_{ex} \approx 2\mathrm{RIN}\frac{\eta}{[1+\eta]^2} I_{\mathrm{DC}}^2 R \quad (20)$$

where $\mathrm{RIN} \approx \sum_n 4\rho_n p_n/(p_S^2 \alpha_S g_A)$ is the relative intensity noise, assumed to be dominated by signal-spontaneous beat noise, of the comb at the output of the EDFA [36]. Finally, the NF can be calculated by the RF gain and the total output noise PSD as

$$\mathrm{NF_{rf}(dB)} = 10\log\left(\frac{\mathrm{N_{out}}}{\mathrm{G_{rf}N_{th}}}\right). \quad (21)$$

III. Simulation

We will now investigate effects of the input split coefficient (α) on the RF performance, when the EDFA output power or output photocurrent is fixed. Fig. 2 shows RF gain, path loss ratio and NF as a function of the input split coefficient α for the fixed output photocurrents of 10, 15, and 20 mA. The EDFA gain is varied to fix the output photocurrents as the input split coefficient is varied. The simulation parameters are summarized in Table I. In Fig. 2(a), as the input split coefficient decreases, RF gain is increased and the interferometer path loss ratio (η) is increased. When the path loss ratio is 0 dB, the input split coefficient is 0.008, producing the highest RF gain at all fixed photocurrents. Then, the RF gain is decreased as the input split coefficient further decreases. This means that the effective optical modulation index related to the power difference between the optical carrier and sideband can be improved by adjusting the path loss ratio. In Fig. 2(b), as the input split coefficient decreases, the NF is decreased with its lowest value occurring at the path loss ratio of 0 dB. Although the path loss ratio of 0 dB produces the highest RF gain, it requires very high output power of the EDFA. For example, the required EDFA output power at the path loss ratio of 0 dB and with a fixed output photocurrent of 20 mA is approximately 39 dBm. In practice, this high EDFA output power may cause damage of the optical components placed after the EDFA.

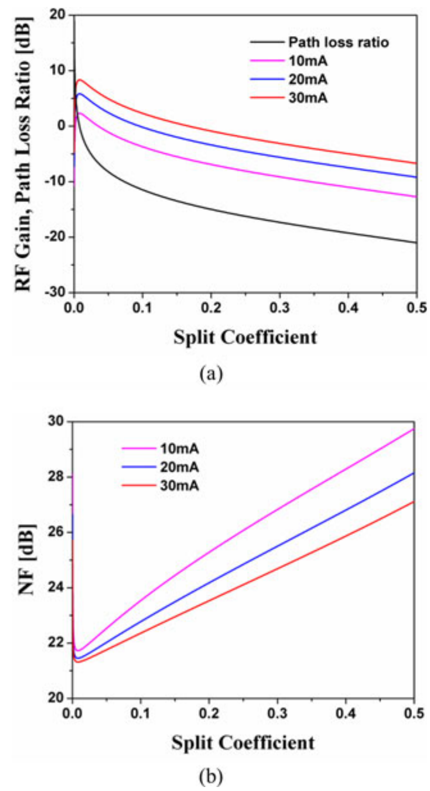

Fig. 2. (a) RF gain, (b) noise figure as a function of the interferometer split coefficient (α) for the fixed output photocurrent of 10, 15, and 20 mA.

TABLE I
SIMULATION PARAMETERS

Parameter	Value	Unit
Half-wave voltage of IM	3	V
Loss of VDL	2.5	dB
Loss of IM	3.5	dB
Extinction ratio of IM	20	dB
Loss of DCF	3.5	dB
Responsivity	0.65	A/W
NF of EDFA	4	dB
RIN of comb source	−170	dB/Hz

Fig. 3 shows the RF gain, output noise, and NF with respect to the input split coefficient for fixed EDFA output power. The EDFA output power is fixed to 31 dBm since the maximum optical power handling of the IM used for this experiment is 30 dBm. The input split coefficient is varied. In Fig. 3(a), the RF gain is maximum at the input split coefficient $\alpha = 0.5$ (i.e.,

$$i_{RF}(t) = \frac{\pi V_{\mathrm{rf}}\kappa\alpha_F\sqrt{\alpha(1-\alpha)\alpha_D\alpha_M}}{2V_\pi}\sum_n p_n\alpha_S g_A\left[\begin{array}{l}\sin\left(\omega_{RF}t+\omega_0\tau+\psi_1\omega_{RF}+\frac{\psi_2}{2}\omega_{RF}^2+n\Delta\omega(\psi_2\omega_{RF}+\tau)\right)\\-\sin\left(\omega_{RF}t-\omega_0\tau+\psi_1\omega_{RF}-\frac{\psi_2}{2}\omega_{RF}^2+n\Delta\omega(\psi_2\omega_{RF}-\tau)\right)\end{array}\right]. \quad (11)$$

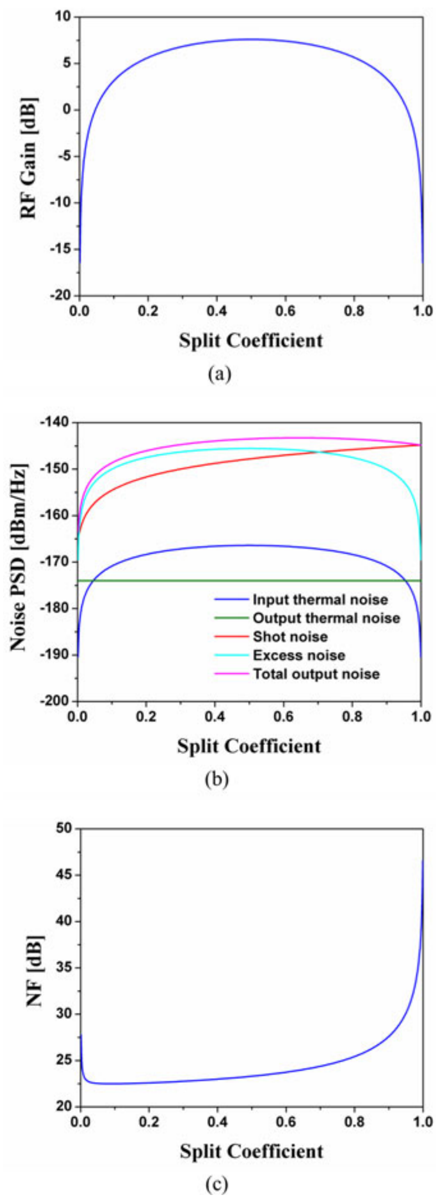

Fig. 3. (a) RF gain, (b) Noise power spectral density, and (c) noise figure as a function of the interferometer input split coefficient for the fixed erbium-doped fiber amplifier output power of 31 dBm.

50:50 input split ratio). Then, the RF gain is reduced as the input split coefficient either increases from 0.5 to 1 or decreases from 0.5 to 0. In Fig. 3(b), the dominant noise terms (shot noise and excess noise) are also reduced as the α decreases from 0.5 towards 0. The RF gain and excess noise in (13) and (19), respectively, have the same factor of $\alpha(1-\alpha)$, related with the input split coefficient. When the excess noise dominates, the NF remains constant as the input split coefficient is varied. However, as shown in Fig. 3(b), when α is large, the shot noise dominates. When the split coefficient α decreases, the shot noise falls more quickly than the excess noise and becomes negligible. Thus, for small α, we may expect excess-noise limited performance. In Fig. 3(c), as the split coefficient decreases from 0.5 to 0.1, the NF improves slightly due to shot noise reduction. This improvement

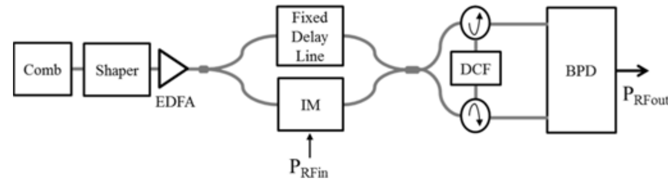

Fig. 4. Experimental configuration A for comparison of two schemes using the single and balanced photodetectors.

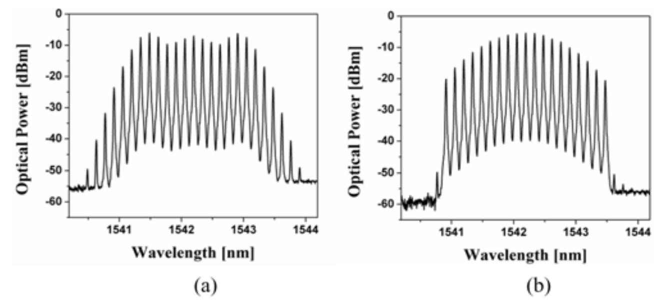

Fig. 5. Spectra of (a) as-generated optical frequency comb and (b) Gaussian-shaped comb.

is similar to that obtained under low biasing in RF photonic links [23], [24].

IV. Experiment

A. Comparison of Filter Using SPD and BPD

Fig. 4 shows the experimental setup for comparison of two schemes using either SPD or BPD. The optical frequency comb with 18 GHz repetition rate and nearly flat power spectrum is generated by cascaded intensity and phase modulation of a continuous-wave laser [21]. Fig. 5(a) shows the spectrum of the optical frequency comb; the resolution bandwidth of the optical spectrum analyzer is 0.02 nm. Then, the amplitude spectrum of the comb is tailored by a commercial optical pulse shaper (Finisar WaveShaper 1000S/SP) to make a Gaussian-shaped comb shown in Fig. 5(b). The Gaussian-shaped comb is amplified by the EDFA and then split into two delay and modulation paths through an optical splitter. We use a 10:90 split ratio achieved with the help of a variable optical attenuator. 10% of the comb is directed to a fixed delay line; 90% of the comb is directed to the IM, which is biased at the minimum transmission point. The IM (EOSPACE AZ-0K5-10) has the half-wave voltage of 4.1 V, the extinction ratio of 30 dB, and RF bandwidth of 10 GHz. The outputs of the fixed delay line and IM are connected to the inputs of a 2×2 optical coupler having a coupling ratio of 50:50. The two outputs of the optical coupler are connected to the BPD through the bidirectional DCF configuration which uses a single spool of DCF and two circulators. The DCF has a dispersion value of −404 ps/nm at 1550 nm. At the inputs of the BPD, a variable optical delay line and variable optical attenuator are used. The BPD (Discovery Semiconductors DSC720-HLPD) is an integrated push-pull device comprised of two InGaAs photodetectors (PD-A and PD-B), with

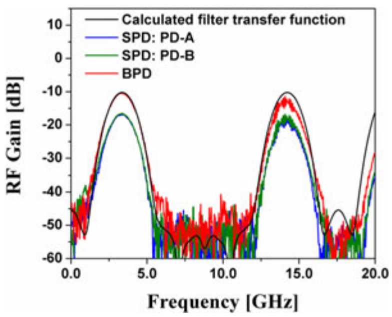

Fig. 6. Measured RF gain and calculated filter transfer function as a function of the RF frequency for two schemes using the single photodetector (PD-A or PD-B) and balanced photodetector.

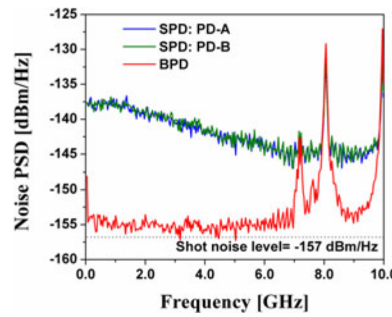

Fig. 7. Noise power spectral density as a function of the RF frequency for two schemes using the single photodetector (PD-A or PD-B) and balanced photodetector.

responsivities of approximately 0.62 and 0.65 A/W. The RF bandwidth of the BPD is approximately 16 GHz. The responsivity of PD-A is lower than that of PD-B by approximately 5%, which corresponds to the common mode rejection ratio of 26 dB. The measured optical power at the inputs of PD-A and PD-B are 10.2 and 10.0 dBm, where the optical powers are intentionally mismatched by approximately 5% to achieve a higher common mode rejection ratio. The total output photocurrent is approximately 13 mA. All RF powers at the output of the BPD are reduced by a factor of 4 since the BPD has an internal matching resistor for maximum power transfer to a matched load. All the numbers shown in this paper for output photocurrent, RF gain, and noise PSD refer to the values before the internal matching resistor. In other words, to account for the internal matching resistor, 6 dB is added to the power measured at the BPD output. To evaluate RF gain, a vector network analyzer is used. For output noise measurements, an electrical spectrum analyzer with a low pass filter and a low noise amplifier is used. The low pass filter (KL Microwaves 6L250-10000/T20000), having a 3-dB cutoff frequency of 10 GHz, is used to suppress the 18 GHz comb beat note. The low noise amplifier (Miteq AMF-4D-001180-24-10P) having the RF gain of >30 dB and the NF of <2.9 dB across 0.1–18 GHz improves the sensitivity of our noise measurements.

We compare the RF performance of the RF photonic filters using the SPD and BPD. For the comparison, we use the results of the scheme using the SPD when only one of the inputs of the BPD is connected. Fig. 6 shows the RF gain as a function of the RF frequency for the two schemes using the SPD (PD-A or PD-B) and BPD. The FSR of the filter is 17.4 GHz. With a delay difference of approximately 10.5 ps between the delay path and modulation path, the RF passband frequencies are 3.33 and 14.07 GHz, the 3 dB bandwidth is approximately 1.3 GHz, and the sidelobe suppression is >30 dB. The RF gain at 3.33 GHz is -16.5 dB for the SPD case (PD-A or PD-B). For the BPD case, the RF gain at 3.33 GHz is -10.3 dB. Compared to the SPD cases, the RF gain of the BPD case is improved by 6 dB because the total output photocurrent is increased by a factor of 2. The filter shape of the BPD case is compared to that of the calculated filter transfer function based on (12) and the Gaussian-shaped comb spectrum shown in Fig. 5(b). At 3.33 GHz, the measured filter shape is closely matched to the calculated transfer function. However, the predicted out-of-band suppression (-43 dB) is approximately 5–10 dB below the simulated value, limited by noise due to spontaneous Brillouin scattering in the DCF. In this experiment total optical power of approximately 15 dBm is injected to the DCF. Since the effective stimulated Brillouin scattering threshold with the comb is high [35], [37], spontaneous Brillouin scattering is dominant and the loss due to the spontaneous Brillouin scattering is negligible [38], [39]. However, the scattering affects the stopband attenuation due to the counterpropagating geometry in the DCF. The RF gain at the 14.07 GHz filter peak for the BPD case interferometer output signals is approximately 2 dB lower than the peak value of the calculated filter transfer function. This difference is attributed to the dependence of the IM half-wave voltage and the BPD responsivities on the RF frequency.

Fig. 7 shows the output noise PSD as a function of RF frequency for the RF photonic filters using the SPD (PD-A or PD-B) and BPD. For the SPD cases, the output noise PSDs are varied in the range of -145.1 to -136.6 dBm/Hz. The dominant noise source is signal-spontaneous beat noise for the SPD case. For the BPD case, the output noise PSD is approximately -155 dBm/Hz with a noise suppression of $10 \sim 18$ dB below 6 GHz. This is close to the shot noise level of approximately -157 dBm/Hz. Because the noise penalty is approximately 2 dB, the excess noise originating from the finite extinction ratio of the IM would be approximately -159.5 dBm/Hz if the suppressed common mode noise is negligible. The NF values for the SPD and BPD cases are approximately 50 and 29 dB at the RF center frequency, respectively. As shown in Fig. 7, noise peaks at the frequencies of approximately 7, 8, and 10 GHz are generated due to the spontaneous Brillouin scattering in the DCF which has multiple resonant peaks in its Brillouin gain spectra [39].

B. Filter Passband Tunability With Enhanced RF Performance

Fig. 8 shows the setup for an experiment which demonstrates both filter passband tunability and enhanced RF performance. Compared to the previous experimental setup, some components have been changed, as has the DCF configuration. First, the filter taps (i.e., the number of comb lines) are increased through the use of an upgraded EO-generated comb generator which

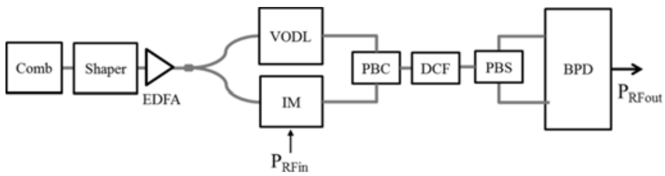

Fig. 8. Experimental configuration B for further RF performance improvement and filter passband tunability. (PBC/PBS: polarization beam combiner/splitter).

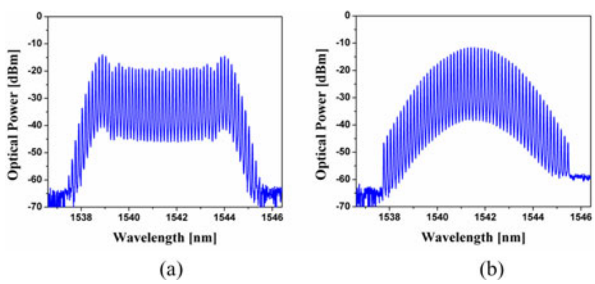

Fig. 9. Optical spectra of (a) EO-generated comb and (b) Gaussian-shaped comb. (Resolution bandwidth = 0.05 nm).

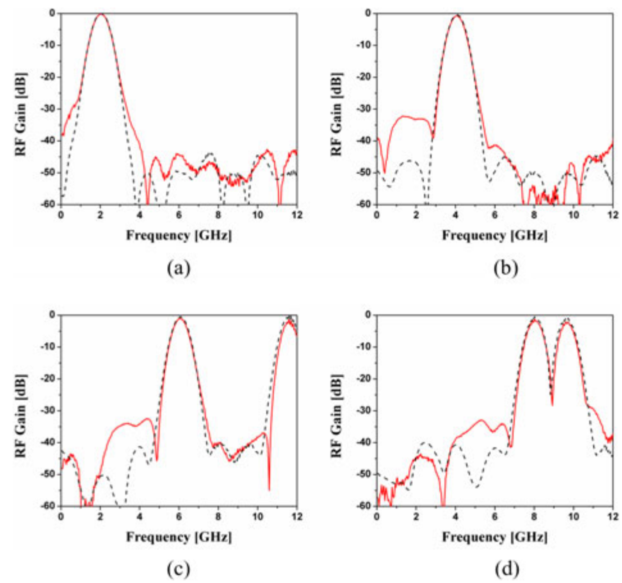

Fig. 10. Measured and simulated RF gain at different filter center frequencies when the center frequencies of lower filter passbands are 2, 4, 6, and 8 GHz. Solid and dash lines indicate measured and simulated values, respectively.

uses three cascaded phase modulators and one IM to generate 60–75 comb lines [22]. The output power of the comb generator is approximately 17 dBm. Fig. 9(a) and (b) shows the generated flat optical frequency comb and Gaussian shaped comb, respectively. The measured relative intensity noise at the output of the EDFA is approximately -152.6 dB/Hz. Second, the fixed delay line is changed to the variable optical delay line for tuning the center frequency of the filter passband. Third, an IM (EOSPACE AZ-1$\times$2-8K8-20) having a lower half-wave voltage (3 V at 1 GHz), higher optical power handling (1 W), and wider RF bandwidth (16 GHz) is used to further increase RF performance. However, the extinction ratio of the IM is 21 dB which is worse than that of the previous IM (extinction ratio = 30 dB). In addition, the output photocurrent is increased to 18.2 mA. Fourth, polarization maintaining fibers and components are used from the comb source to the interferometer. The EDFA has an internal polarizer so the amplified spontaneous emission noise at its output is polarized. Finally, the bidirectional DCF configuration was changed to the polarization multiplexing DCF configuration to solve the Brillouin scattering problem. In Fig. 8, the delay and modulation path signals at the output of the interferometer are orthogonally combined by a polarization beam combiner. The output signal is transmitted through the DCF to a polarization beam splitter. The principal axes of the polarization beam splitter are aligned to have an angle of 45° to the polarization state of either the delay or modulation path signal for generation of complementary signals. The complementary signals are detected by the BPD. In the polarization multiplexing DCF configuration, the effects of the Brillouin scattering on the filter transfer function and noise peaks is minimized because the propagation direction in the DCF is unidirectional, whereas Brillouin scattering occurs in the counterpropagating direction. Therefore, care should be taken to avoid reflection of the generated Brillouin scattering noise.

Fig. 10 shows the measured and simulated RF gain when the center frequencies of lower filter passbands are 2, 4, 6, and 8 GHz. Because of the increased number of comb lines, the 3 dB bandwidth is decreased to approximately 770 MHz. The measured RF gain values at the filter peaks are varied from 0 to -1.3 dB, which are higher than that of the previous setup due to the lower half-wave voltage and increased output photocurrent. The measured RF gain and filter transfer function agree well with the simulated values. The sidelobe suppression is >32 dB. The stopband attenuation on the high frequency side of the primary passband is in the range 40–55 dB. The baseband response caused by the residual optical carriers in the modulation path is suppressed by balanced detection. However, some baseband response remains due to the finite common mode rejection ratio, and this baseband response varies due to bias drift of the IM. At baseband, the RF gain is lower than approximately -38 dB. Fig. 11 shows measured and simulated noise PSD as a function of the frequency at different filter center frequencies of 2, 4, 6, and 8 GHz. The estimated shot noise is -155.4 dBm/Hz at the total output photocurrent of 18.2 mA. Using (17) and (20), the calculated total output noise and excess noise are -150.3 and -152 dBm/Hz, respectively. Above 2 GHz, the measured output noise levels are flat and their average values are very close to the simulated value. The noise penalty of this setup is approximately 5 dB, which is higher than that of the previous setup due to the lower extinction ratio of the IM and increased output photocurrent. As the filter passband is tuned from 2 to 8 GHz, the measured output noise levels are not changed. Fig. 12 shows measured and simulated NF as a function of the filter center frequencies. The measured NF values estimated by (21) are from 24 to 26 dB. The difference values between the measured and

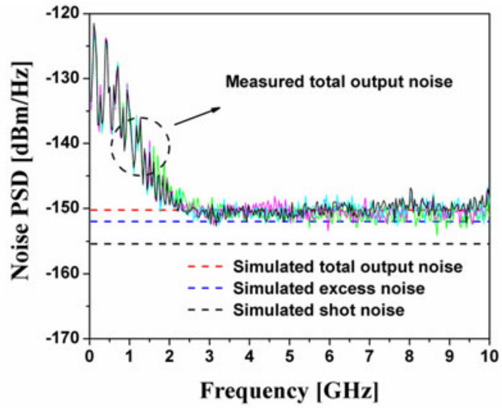

Fig. 11. Measured and simulated noise power spectral densities as a function of the frequency at different filter center frequencies of 2, 4, 6, and 8 GHz.

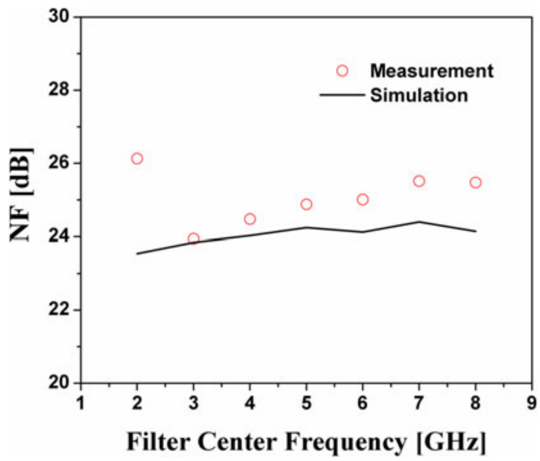

Fig. 12. Measured and simulated noise figure as a function of the filter center frequency.

TABLE II
RF PERFORMANCE COMPARISON

Schemes		RF gain(dB)	NF(NP)(dB)	$^*V_\pi$ (V)	ER(dB)	I_{DC} (mA)
Filtering [15]		−40	–	–	–	0.9
Experiment-A (This work)	SPD	−16.5	50	4.1	30	6.5
	BPD	−10.3	29 (2)			13
Experiment-B (This work)		−1.3 ∼ 0	24 ∼ 26 (5)	3	21	18.2
**Conventional link [24]		−0.42	19.1 (0)	3	–	18.2

* All values are at 1 GHz.
** Simulation results with a dual-output modulator and a balanced photodetector.
NP: noise penalty ($= 10\log(N_{out}/N_{shot})$); ER: extinction ratio.

simulated NF are less than approximately 1.4 dB for the filter peaks of 3 to 8 GHz. However, at the filter peak of 2 GHz, the difference value of 2.6 dB is relatively higher than those of the other filter peaks due to the low-frequency interferometric noise shown in Fig. 11. It is attributed to continuous-wave laser phase- to intensity-noise conversion which takes place in the DCF-PBS of this scheme [40]–[42]. The low-frequency noise could be eliminated using a unidirectional DCF configuration which has two well-matched DCFs. However, from a practical perspective, the fabrication of two DCFs with precisely the same delay and dispersion values is difficult, and stabilization may be required; any mismatches degrade the common mode rejection ratio for balanced detection. A multi-core fiber or an optical ribbon could potentially be used because the fiber cores or multiple fibers are made with a single cladding or ribbon package, respectively, which should provide for stable matching between the different cores [43], [44].

The overall RF performance of the RF photonic filter using the BPD is substantially improved as compared to the conventional filtering schemes. Table II compares experimental results of the filtering schemes and simulation results of the conventional link with the noise reduction technique using a dual-output modulator and a BPD. Compared to [15] and the experiment-A, the RF gain of the experiment-B is increased to approximately 0 dB due to the lower-V_π and increased photocurrent. It is comparable to that of the conventional link at the same V_π and photocurrent. The NF of the RF photonic filter is improved to approximately 24 dB. However, the noise penalty is degraded from 2 to 5 dB due to the lower extinction ratio and increased photocurrent. In the experiment-B, with the extinction ratio of >26 dB, the noise penalty can be further reduced to approximately 0 dB and thus the NF of the RF photonic filter would become also close to that of the conventional link.

V. CONCLUSION

We demonstrate improvements to the RF performance of comb-based RF photonic filters by using an interferometric configuration with DSB-SC and balanced detection. Balanced detection increases the output photocurrent by a factor of two and thus improves the RF gain by 6 dB. Intensity noise is suppressed both through biasing the intensity modulator inside the interferometer at the minimum transmission point and through balanced detection, resulting in the reduction of the noise figure. In addition, we show how the effective optical modulation index and NF can be improved by adjusting the input split ratio of the interferometer. In a first experiment using a balanced photodetector (BPD) and a counterpropagating geometry in a dispersive fiber, we achieve a RF gain of −10.3 dB and a NF of 29 dB at the filter center frequency. Compared to an identical experiment but using a single photodiode, the RF gain and NF are improved by approximately 6 and 21 dB, respectively. In a second experiment using an intensity modulator with lower half-wave voltage, an increased output photocurrent, and a copropagating polarization multiplexing geometry in a dispersive fiber, the RF gain and NF are further improved up to approximately 0 and 24 dB, respectively. In the latter experiment the filter passband is tuned from 2 to 8 GHz while maintaining roughly constant RF gain and noise figure, without RF power fading, without filter baseband response, and with approximately Gaussian RF filter shape (maintaining sidelobe suppression and stopband attenuation >32 dB). We believe that the RF performance metrics such as RF gain and NF can be further improved through the use of a high-power, low-noise continuous-wave laser as a seed to the electro-optic comb generator and through the use of an intensity modulator having lower half-wave voltage and higher extinction ratio.

An additional dimension important to pursue for practical applications is to increase the level of integration. In another paper to appear in this special issue [45], our group has demonstrated programmable RF photonic filtering using a comb source generated via CW-laser pumping of an on-chip silicon nitride microresonator. Optical pulse shaping has been demonstrated at the chip-level by several groups in platforms such as InP, silica, and silicon, e.g., [46]–[49]. Although significant further work is needed, such developments suggest the potential for substantial reduction in the footprint of RF photonic filters employing optical frequency combs.

Acknowledgment

The authors would like to thank helpful discussions with J. D. McKinney and V. R. Supradeepa.

References

[1] J. Uher and W. J. R. Hoefer, "Tunable microwave and millimeter-wave band-pass filters," *IEEE Trans. Microw. Theory Tech.*, vol. 39, no. 4, pp. 643–653, Apr. 1991.
[2] G. M. Rebeiz, *RF MEMS: Theory, Design, and Technology*. Hoboken, NJ, USA: Wiley, 2003.
[3] S. J. Park, I. Reines, C. Patel, and G. M. Rebeiz, "High-Q RF-MEMS 4–6-GHz tunable evanescent-mode cavity filter," *IEEE Trans. Microw. Theory Tech.*, vol. 58, no. 2, pp. 381–389, Feb. 2010.
[4] X. Liu, L. P. B. Katehi, W. J. Chappell, and D. Peroulis, "High-Q tunable microwave cavity resonators and filters using SOI-based RF MEMS tuners," *IEEE J. Microelectromech. Syst.*, vol. 19, no. 4, pp. 774–784, Aug. 2010.
[5] E. J. Naglich, J. Lee, D. Peroulis, and W. J. Chappell, "Switchless tunable bandstop-to-all-pass reconfigurable filter," *IEEE Trans. Microw. Theory Tech.*, vol. 60, no. 5, pp. 1258–1265, May 2012.
[6] J. Capmany, B. Ortega, and D. Pastor, "A tutorial on microwave photonic filters," *J. Lightw. Technol.*, vol. 24, no. 1, pp. 201–229, Jan. 2006.
[7] J. Capmany, D. Pastor, and B. Ortega, "New and flexible fiber-optic delay line filters using chirped Bragg gratings and laser arrays,"*IEEE Trans. Microw. Theory Tech.*, vol. 47, no. 7, pp. 1321–1327, Jul. 1999.
[8] Y. Dai and J. Yao, "Nonuniformly-spaced photonic microwave delayline filter," *Opt. Exp.*, vol. 16, no. 7, pp. 4713–4718, Mar. 2008.
[9] L. Li, X. Yi, T. X. H. Huang, and R. A. Minasian, "Distortion-free spectrum sliced microwave photonic signal processor: analysis, design and implementation," *Opt. Exp.*, vol. 20, no. 10, pp. 11517–11528, May 2012.
[10] J. Mora, B. Ortega, J. Capmany, J. L. Cruz, M. V. Andres, D. Pastor, and S. Sales, "Automatic tunable and reconfigurable fiberoptic microwave filters based on a broadband optical source sliced by uniform ber Bragg gratings," *Opt. Exp.*, vol. 10, no. 22, pp. 1291–1298, Nov. 2002.
[11] A. Ortigosa-Blanch, J. Mora, J. Capmany, B. Ortega, and D. Pastor, "Tunable radio-frequency photonic filter based on an actively mode locked fiber laser," *Opt. Lett.*, vol. 31, no. 6, pp. 709–711, Mar. 2006.
[12] E. Hamidi, R. Wu, V. R. Supradeepa, C. M. Long, D. E. Leaird, and A. M. Weiner, "Tunable radio frequency photonic filter based on intensity modulation of optical combs," in *Proc. IEEE Top. Meeting Microw. Photon.*, Oct. 2010, pp. 393–396.
[13] E. Hamidi, D. E. Leaird, and A. M. Weiner, "Tunable programmable microwave photonic filters based on an optical frequency comb," *IEEE Trans. Microw. Theory Tech.*, vol. 58, no. 11, pp. 3269–3278, Nov. 2010.
[14] M. Song, C. M. Long, R. Wu, D. Seo, D. E. Leaird, and A. M. Weiner, "Reconfigurable and tunable flat-top microwave photonic filters utilizing optical frequency comb," *IEEE Photon. Technol. Lett.*, vol. 23, no. 21, pp. 1618–1620, Nov. 2011.
[15] V. R. Supradeepa, C. M. Long, R. Wu, F. Ferdous, E. Hamidi, D. E. Leaird, and A. M. Weiner, "Comb-based radio-frequency photonic filters with rapid tunability and high selectivity," *Nature Photon.*, vol. 6, pp. 186–194, 2012.
[16] M. Song, V. Torres-Company, A. J. Metcalf, and A. M. Weiner, "Multitap microwave photonic filters with programmable phase response via optical frequency comb shaping," *Opt. Lett.*, vol. 37, pp. 845–847, Mar. 2012.
[17] R. Wu, C. M. Long, D. E. Leaird, and A. M. Weiner, "Directly generated Gaussian-shaped optical frequency comb for microwave photonic filtering and picosecond pulse generation," *IEEE Photon. Techn. Lett.*, vol. 24, no. 17, pp. 1484–1486, Sep. 2012.
[18] M. Song, V. Torres-Company, R. Wu, A. J. Metcalf, and A. M. Weiner, "Compression of ultra-long microwave pulses using programmable microwave photonic phase filtering with >100 complex-coefficient taps," *Opt. Exp.*, vol. 22, no. 6, pp. 6329–6338, 2014.
[19] R. Wu, M. Song, D. E. Leaird, and A. M. Weiner, "Comb-based radio-frequency photonic filtering with 20 ns bandwidth reconfiguration," *Opt. Lett.*, vol. 38, no. 15, pp. 2735–2738, 2013.
[20] V. Torres-Company, D. E. Leaird, and A. M. Weiner, "Simultaneous broadband microwave downconversion and programmable complex filtering by optical frequency comb shaping," *Opt. Lett.*, vol. 37, no. 19, pp. 3993–3995, 2012.
[21] R. Wu, V. R. Supradeepa, C. M. Long, D. E. Leaird, and A. M. Weiner, "Generation of very flat optical frequency combs from continuous wave lasers using cascaded intensity and phase modulators driven by tailored radio frequency waveforms," *Opt. Lett.*, vol. 35, no. 19, pp. 3234–3236, Oct. 2010.
[22] A. J. Metcalf, V. Torres-Company, D. E. Leaird, and A. M. Weiner, "High-power broadly tunable electro-optic frequency comb generator," *IEEE J. Sel. Topics Quantum Electron.*, vol. 19, no. 6, pp. 3500306–3500306, Nov./Dec. 2013.
[23] C. Cox, E. Ackerman, G. Betts, and J. Prince, "Limits on the performance of RF-over-fiber links and their impact on device design," *IEEE Trans. Microw. Theory Tech.*, vol. 54, no. 2, pp. 906–920, Feb. 2006.
[24] E. I. Ackerman, G. E. Betts, W. K. Burns, J. C. Campbell, C. H. Cox, N. Duan, J. L. Prince, M. D. Regan, and H. V. Roussell, "Signal-to-noise performance of two analog photonic links using different noise reduction techniques," in *Proc. IEEE MTT-S Int. Microw. Symp. Dig.*, Jun. 2007, pp. 51–54.
[25] J. D. McKinney, M. Godinez, V. J. Urick, S. Thaniyavarn, W. Charczenko, and K. J. Williams, "Sub-10 dB noise figure in a multiple-GHz analog optical link," *IEEE Photon. Technol. Lett.*, vol. 19, no. 7, pp. 465–467, Apr. 2007.
[26] I. Gasulla and J. Capmany, "Analytical model and figures of merit for filtered microwave photonic links," *Opt. Exp.*, vol. 19, no. 20, pp. 19758–19774, Sep. 2011.
[27] M. Bolea, J. Mora, B. Ortega, and J. Capmany, "Highly chirped single-bandpass microwave photonic filter with reconfiguration capabilities," *Opt. Exp.*, vol. 19, no. 5, pp. 4566–4576, 2011.
[28] X. Xue, X. Zheng, H. Zhang, and B. Zhou, "Highly reconfigurable microwave photonic single-bandpass filter with complex continuous time impulse responses," *Opt. Exp.*, vol. 20, no. 24, pp. 26929–26934, 2012.
[29] X. Xue, X. Zheng, H. Zhang, and B. Zhou, "Spectrum-sliced microwave photonic filter with an improved dynamic range based on a $LiNbO_3$ phase modulator and balanced detection," *IEEE Photon. Techn. Lett.*, vol. 24, no. 9, pp. 775–777, May 2012.
[30] X. Xue, X. Zheng, H. Zhang, and B. Zhou, "Noise reduction by balanced detection in microwave photonic filters based on optical broadband sources," in *Proc. Conf. Lasers Electro-Opt.*, 2011, pp. 1–3, Paper CThY3.
[31] H.-J. Kim, D. E. Leaird, and A. M. Weiner, "Improved RF performance of a comb-based microwave photonic filter using a balanced photodetector," in *Proc. IEEE Top. Meeting Microw. Photon.*, Oct. 2013, pp. 80–83.
[32] C. Middleton and R. Desalvo, "High performance microwave photonic links using double sideband suppressed carrier modulation and balanced coherent heterodyne detection," in *Proc. IEEE Mil. Commun. Conf.*, 2009, pp. 1–6.
[33] V. J. Urick, M. S. Rogge, F. Bucholtz, and K. J. Williams, "The performance of analog photonic links employing highly compressed erbium-doped fiber amplifiers," *IEEE Trans. Microw. Theory Tech.*, vol. 54, no. 7, pp. 3141–3145, Jul. 2006.
[34] A. M. Weiner, *Ultrafast Optics*, 1st ed. New York, NY, USA: Wiley, 2009.
[35] J. D. McKinney and K. J. Williams, "Sampled analog optical links," *IEEE Trans. Microw. Theory Tech.*, vol. 57, no. 8, pp. 2093–2099, Aug. 2009.
[36] D. Derickson, *Fiber Optic Test and Measurement*. Englewood Cliffs, NJ, USA: Prentice-Hall, 1998.

[37] J. D. McKinney, V. J. Urick, and J. Briguglio, "Optical comb sources for high dynamic-range single-span long-haul analog optical links," *IEEE Trans. Microw. Theory Tech.*, vol. 59, no. 12, pp. 3249–3257, Dec. 2011.

[38] A. Kobyakov, M. Sauer, and D. Chowdhury, "Stimulated Brillouin scattering in optical fibers," *Adv. Opt. Photon.*, vol. 2, no. 1, pp. 1–59, 2010.

[39] A. Yeniay, J. Delavaux, and J. Toulouse, "Spontaneous and stimulated Brillouin scattering gain spectra in optical fibers," *J. Lightw. Technol.*, vol. 20, no. 8, pp. 1425–1432, Aug. 2002.

[40] W. K. Marshall, B. Crosignani, and A. Yariv, "Laser phase noise to intensity noise conversion by lowest-order group-velocity dispersion in optical fiber: Exact theory," *Opt. Lett.*, vol. 25, no. 3, pp. 165–167, Feb. 2000.

[41] J. C. Attard, J. E. Mitchell, C. J. Rasmussen, "Performance analysis of interferometric noise due to unequally powered interferers in optical networks," *J. Lightw. Technol.*, vol. 23, no. 4, pp. 1692–1703, Apr. 2005.

[42] R. W. Tkach and A. R. Chraplyvy, "Phase noise and linewidth in an InGaAsP DFB laser," *J. Lightw. Technol.*, vol. 4, no. 11, pp. 1711–1716, Nov. 1986.

[43] T. Hayashi, T. Taru, O. Shimakawa, T. Sasaki, and E. Sasaoka, "Low-crosstalk and low-loss multi-core fiber utilizing fiber bend," presented at the Opt. Fiber Commun. Conf. Expo., Los Angeles, CA, USA, 2011, Paper OWJ3.

[44] G. S. Brockway and M. R. Santana, "Analysis of thermally induced loss in fiber-optic ribbons," *Bell Syst. Tech. J.*, vol. 62, no. 4, pp. 993–1018, Apr. 1983.

[45] X. Xue, Y. Xuan, H.-J. Kim, J. Wang, D. E. Leaird, M. Qi, and A. M. Weiner, "Programmable single-bandpass photonic RF filter based on Kerr comb from a microring," *J. Lightw. Technol*., vol. PP, no. 99, pp. 1, Mar. 2014.

[46] M. J. R. Heck, P. Munoz, B. W. Tilma, E. A. J. M. Bente, Y. Barbarin, Y.-S. Oei, R. Notzel, and M. K. Smit, "Design, fabrication and characterization of an InP-based tunable integrated optical pulse shaper," *IEEE J. Quantum Electron.*, vol. 44, no. 4, pp. 370–377, Apr. 2008.

[47] S. Tahvili, S. Latkowski, B. Smalbrugge, X. J. M. Leijtens, P. J. Williams, M. J. Wale, J. Parra-Cetina, R. Maldonado-Basilio, P. Landais, M. K. Smit, E. A. J. M. Bente, "InP-based integrated optical pulse shaper: Demonstration of chirp compensation," *IEEE Photon. Technol. Lett.*, vol. 25, no. 5, pp. 450–453, Mar. 2013.

[48] D. J. Geisler, N. K. Fontaine, T. He, R. P. Scott, L. Paraschis, J. P. Heritage, and S. J. B. Yoo, "Modulation-format agile, reconfigurable Tb/s transmitter based on optical arbitrary waveform generation," *Opt. Exp.*, vol. 17, no. 18, pp. 15911–15925, 2009.

[49] M. H. Khan, H. Shen, Y. Xuan, L. Zhao, S. Xiao, D. E. Leaird, A. M. Weiner, and M. Qi, "Ultrabroad-bandwidth arbitrary radiofrequency waveform generation with a silicon photonic chip-based spectral shaper," *Nature Photon.*, vol. 4, no. 2, pp. 117–122, 2010.

Hyoung-Jun Kim received the B.S. degree in electrical engineering from Kwangwoon University, Seoul, Korea, in 2005. He received the M.S. and Ph.D. degrees in electrical engineering from Gwangju Institute of Science and Technology, Gwangju, Korea, in 2007 and 2011, respectively.

From 2011 to 2012, he was at High Speed Integrated Circuit Laboratory in GIST, where he was engaged in research on millimeter-wave communication systems utilizing RF photonics technologies. In 2012, he joined the Ultrafast Optics group in Purdue University, USA, where he is currently working on reconfigurable RF photonic filters based on optical frequency combs and optical pulse shaping.

Daniel E. Leaird was born in Muncie, IN, USA, in 1964. He received the B.S. degree in physics from Ball State University, Muncie, IN, in 1987, and the M.S. and Ph.D. degrees from the School of Electrical and Computer Engineering, Purdue University, West Lafayette, IN, in 1996 and 2000, respectively.

He joined Bell Communications Research (Bellcore), Red Bank, NJ, USA, as a Senior Staff Technologist in 1987, and later advanced to Member of Technical Staff. From 1987 to 1994, he worked in the Ultrafast Optics and Optical Signal Processing Research Group, where he was a key team member in research projects in ultrafast optics, such as shaping of short optical pulses using liquid crystal modulator arrays, investigation of dark soliton propagation in optical fibers, impulsive stimulated Raman scattering in molecular crystals, and all-optical switching.

Dr. Leaird is currently a Senior Research Scientist and Laboratory Manager of the Ultrafast Optics and Optical Fiber Communications Laboratory, School of Electrical and Computer Engineering, Purdue University, where he has been since 1994. He has coauthored approximately 100 journal articles, 150 conference proceedings, and has three issued U.S. patents.

He is active in the optics community and professional organizations including the Optical Society of America and IEEE Photonics Society where he served as the Chair of the Ultrafast Optics technical committee from 2006–2009 as well as serving as a Consultant to venture capitalists by performing technical due diligence. He also serves as a Reviewer for *Optics Letters*, *Optics Express*, *Photonics Technology Letters*, *Applied Optics*, and *Journal of the Optical Society of America B* in addition to serving on National Science Foundation review panels in the SBIR program.

Dr. Leaird received several awards for his work in the ultrafast optics field including a Purdue Professional Achievement Award, a Magoon Award for outstanding teaching, an Optical Society of America/New Focus Student Award, and a Bellcore "Award of Excellence."

Andrew J. Metcalf received the B.S. degree (*summa cum laude*) in electrical engineering from the University of Wisconsin-Milwaukee, Milwaukee, WI, USA, in 2010, and the M.S.E.C.E degree from Purdue University, West Lafayette, IN, USA, in 2012, where he is currently working toward the Ph.D. degree in electrical engineering.

From 2008–2010, he worked as a co-op at Harley-Davidson Motor Company before becoming a Graduate Research Assistant in the Ultrafast Optics and Optical Fiber Communications group at Purdue. For his undergrad work, he received the Deans Award for outstanding achievement in electrical and computer engineering. He is a Member of both OSA and IEEE, and serves as a Reviewer for *Optics Letters*, *Optics Express*, and *Photonics Technology Letters*. His research interests include optical pulse shaping, frequency comb generation, and radio-frequency photonics.

Andrew M. Weiner received the Sc.D. degree in electrical engineering from the Massachusetts Institute of Technology, Cambridge, MA, USA, in 1984. He is the Scifres Family Distinguished Professor of Electrical and Computer Engineering. In 2008, he was elected to membership in the National Academy of Engineering and in 2009 was named a Department of Defense National Security Science and Engineering Faculty Fellow. He recently served a three year term as the Chair of the National Academy's U.S. Frontiers of Engineering Meeting; he is currently serving as an Editor-in-Chief of Optics Express, an all-electronic, open access journal publishing more than 3000 papers a year emphasizing innovations in all aspects of optics and photonics. He joined Bellcore, at that time a premier telecommunications industry research organization, first as Member of Technical Staff and later as a Manager of Ultrafast Optics and Optical Signal Processing Research. He joined Purdue as a Professor in 1992, and has since graduated more than 30 Ph.D. students. He has also spent sabbaticals at the Max Born Institute for Nonlinear Optics and Ultrashort Pulse Spectroscopy, Berlin, Germany, and at JILA, University of Colorado and National Institute of Standards and Technology, Boulder, CO, USA.

His research interests include ultrafast optics, with a focus on processing of extremely high speed lightwave signals. He is especially well known for his pioneering work on programmable generation of arbitrary ultrashort pulse waveforms, which has found application both in fiber optic networks and in ultrafast optical science laboratories around the world.

Prof. Weiner is the author of a textbook entitled *Ultrafast Optics*, has published eight book chapters and more than 270 journal articles, and is inventor of 15 U.S. patents. His numerous awards include the Hertz Foundation Doctoral Thesis Prize in 1984, the Optical Society of America's Adolph Lomb Medal in 1990, and R.W. Wood Prize in 2008, the International Commission on Optics Prize in 1997, and the IEEE Photonics Society's William Streifer Scientific Achievement Award in 1999 and Quantum Electronics Prize in 2011. At Purdue, he has been recognized with the inaugural Research Excellence Award from the Schools of Engineering in 2003, the Provost's Outstanding Graduate Student Mentor Award in 2008, and the Herbert Newby McCoy Award for outstanding contributions to the natural sciences in 2013.